

Looking Inside the Widom Region: Non-Equilibrium Stratification in Supercritical CO₂

Paul Fruton^{1,2}, Emma Lisoir^{1,3,4}, Happiness Imuetinyan^{1,5}, Cédric Giraudet^{1,6},
Fabrizio Croccolo¹

¹Universite de Pau et des Pays de l'Adour, E2S UPPA, CNRS, LFCR, 64600 Anglet,
France.

²Dipartimento di Fisica 'A. Pontremoli', Università degli Studi di Milano, 20133 Milano,
Italy.

³Univ Toulouse, INSA Toulouse, CNRS, LPCNO, Toulouse, France.

⁴Laboratoire de Génie Chimique, CNRS, Toulouse INP, Université de Toulouse,
Toulouse, France.

⁵Universite de Pau et des Pays de l'Adour, E2S UPPA, CNRS, LFCR, 64000 Pau, France.

⁶Currently with CTS Consulting & Technical Support, 27200 Vernon, France.

Contributing authors: fabrizio.croccolo@univ-pau.fr;

Abstract

The supercritical state of matter is usually described as a continuous phase without sharp boundaries between liquid and gas regions. However, under non-equilibrium conditions, this view breaks down. Here we report an experimental investigation of non-equilibrium fluctuations in supercritical carbon dioxide (CO₂) subjected to a stabilising temperature gradient. Using shadowgraphy, we reveal spontaneous stratification of the fluid into different layers, separated by transition regions, where thermodynamic properties vary dramatically. These signatures are particularly evident when the system crosses the Widom lines, loci of the extrema of the response function in the supercritical domain [1–3]. The analysis of the intermediate scattering function of temperature fluctuations highlights the presence of Brunt–Väisälä oscillations within the fluid at multiple frequencies. These oscillations arise from the coupling of thermal and viscous modes under gravity [4–6] and are a clear signature of the layered structure of the fluid. Our approach enables systematic exploration of a wide range of thermodynamic conditions in a single experiment. These findings suggest that the Widom region cannot be described as a homogeneous phase, but rather as a dynamic assembly of phase-like behaviours, challenging the applicability of classical thermodynamics in non-equilibrium supercritical regimes.

Keywords: supercritical fluids, phase behaviour, shadowgraphy, Widom lines

Commonly, the supercritical phase is referred to as a phase that is neither gas nor liquid, where the fluid properties vary smoothly from those of a gas to those of a liquid. This combination allows a supercritical fluid to exhibit properties of both

phases, such as the high density of the liquid phase and the low viscosity of the gas one, making the supercritical state of great interest for many industrial applications. A suitable example is the transport of supercritical CO₂ through

pipelines, where its high density allows efficient fluid transfer, while its low viscosity minimises energy consumption.

This theoretical description holds under equilibrium conditions, but fluids in the real world are only exceptionally at equilibrium, because almost every industrial application features inhomogeneities in the thermodynamic variables, leading the fluid out of equilibrium. An additional question is: can a fluid out of equilibrium be used to test different points of the phase diagram as if the superposition of distinct equilibrium points?

Regarding the description of the supercritical state, the concept of Widom lines has emerged in recent decades as a way to describe the loci of maxima in response functions, such as heat capacity, compressibility, or sound speed, extending into the supercritical region from the critical point [7, 8]. Although this viewpoint is debated, Widom lines are increasingly recognised as boundaries between regimes of liquid- and gas-like behaviour [9–11]. Their significance, however, has rarely been tested under non-equilibrium conditions. Moreover, the equilibrium perspective neglects the role of fluctuations, which are ubiquitous in fluid systems, even under equilibrium conditions, and become increasingly important in the vicinity of the critical point or in the presence of a macroscopic gradient [4, 12].

Indeed, in a pure fluid stressed by a thermal gradient, giant nonequilibrium fluctuations (NEFs) take place at all possible spatial scales, or equivalently, wave numbers. NEFs are largely amplified by the coupling between vertical velocity fluctuations and the macroscopic gradient and are limited only by gravity or the finite size of the sample [13–16]. In this study, we focus on the intermediate scattering function (ISF) of temperature fluctuations, which characterizes their dynamics and the corresponding time evolution, providing an efficient insight into the processes that take place within the fluid [5, 17].

A pure subcritical fluid placed out of equilibrium by a stabilizing thermal gradient far from the critical point shows constant thermal diffusivity α_T . In this case, the ISF of thermal fluctuations can be modelled by a simple exponential decay, termed the thermal mode

$$f(q, dt) = \exp\left(-\frac{dt}{\tau(q)}\right). \quad (1)$$

The decay time $\tau(q)$ depends both on thermal diffusivity and gravity [4, 12, 18–20]

$$\tau(q) = \frac{1}{\alpha_T q^2 \left[1 + \left(\frac{q_{ro,T}}{q} \right)^4 \right]}, \quad (2)$$

where $q_{ro,T}$ is the characteristic roll-off wave number at which diffusion of temperature and gravity act on similar timescales [5, 17]

$$q_{ro,T} = \left(-\frac{\beta_T \vec{g} \cdot \vec{\nabla}T}{\alpha_T \nu} \right)^{1/4} = \frac{(-\text{Ra})^{1/4}}{L}, \quad (3)$$

where $\beta_T = -(1/\rho) (\partial \rho / \partial T)_p$ is the isobaric thermal expansion coefficient, \vec{g} the acceleration of gravity, $\vec{\nabla}T$ the temperature gradient across the sample, α_T the thermal diffusivity, ν the kinematic viscosity, Ra the Rayleigh number and L the thickness of the fluid layer.

Large fluctuations ($q \ll q_{ro,T}$) relax faster by buoyancy, while small ones ($q \gg q_{ro,T}$) vanish faster by thermal conduction [4, 12]. At wave numbers much smaller than $q_{ro,T}$, a more complete model derived by fluctuating hydrodynamic theory [4, 21] predicts the existence of a propagating mode at low q , i.e. $q < q_p = \frac{1}{L} \left(-\frac{4\text{Ra}}{(\text{Pr}-1)^2} \right)^{1/4}$, with $\text{Pr} = \nu/\alpha_T$ the Prandtl number. In this case, the ISF can be modelled by

$$f(q, dt) = \frac{\cos(\Omega dt + \phi)}{\cos(\phi)} \exp\left(-\frac{dt}{\tau(q)}\right) \quad (4)$$

where $\tau(q)$ is the decay time and $\Omega(q)$ is the oscillation frequency whose maximum Ω_{\max} corresponds to the Brunt-Väisälä frequency

$$\Omega_{\max} = \sqrt{\vec{g} \cdot \vec{\nabla}\rho/\rho} = \sqrt{\beta_T \vec{g} \cdot \vec{\nabla}T}, \quad (5)$$

as fluctuations can be assimilated to a body oscillating in a stratified volume [4, 6, 21]. Long-range correlated fluctuations oscillate within the sample, while those correlated over smaller distances decay either by buoyancy or diffusion without oscillating, as already observed in liquid mixtures of two or three components for temperature and concentration fluctuations [15, 21, 22].

Here, we use high-sensitivity shadowgraph setup to investigate temperature non-equilibrium fluctuations in supercritical CO₂ layers subjected

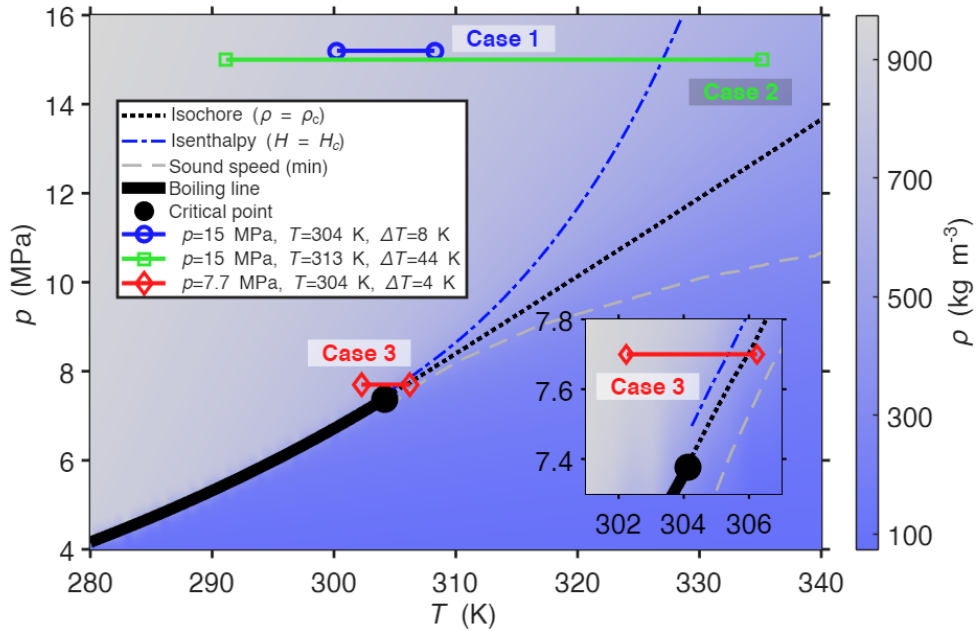


Fig. 1 Density map of pure CO₂ in the *p*-*T* diagram. Indications of the Widom region limits are provided by the minimum sound speed line (dashed gray line) and the isenthalpy line (dashed and dotted blue line), while the isochore is displayed as well (dashed dark line). The thermal gradients corresponding to the experiments analysed and discussed here are displayed with solid horizontal segments. Inset: close-up of the *p*-*T* diagram around the critical point.

to vertical stabilising temperature gradients. This method has previously been applied to critical fluids and polymer solutions to study giant fluctuations, transport coefficients, and convection under gravity [12, 23]. Challenging measurements have also been performed under microgravity conditions due to the robustness of the dynamic shadowgraph approach [24].

Using our methodology [5], we analyse density 2D-maps in the Fourier space, thus separating the signal at different wave numbers *q*. By means of the Differential Dynamic Algorithm [5, 17], whose concept is illustrated in Fig. 2, we compute the structure functions (SFs) of fluid density fluctuations, captured by shadowgraphy, integrated over the vertical axis, parallel to the temperature gradient. The SFs contain quantitative information on the evolution of NEFs in both time and space, according to the following equation:

$$SF(q, dt) = 2\{S(q) T(q)[1 - f(q, dt)] + B(q)\}, \quad (6)$$

where *S*(*q*) is the NEF static structure function, *T*(*q*) is the shadowgraph transfer function, *f*(*q*, *dt*) is the ISF and *B*(*q*) is a noise term [23].

We use a specialised high-pressure cell (HP) to investigate temperature fluctuations in a layer of pure CO₂ stressed by a stabilising temperature gradient. Details on the HP cell and optical setup can be found in the Methods section and in previous publications [25].

Here we report the results of three significant experiments with different average temperatures, pressures, and temperature gradients, as shown in Fig. 1, where the limits of the Widom region, defined by the minimum speed-of-sound line and the isenthalpy line, are also reported. The colour-code additionally shows the different values of the fluid density as calculated based on NIST data [26].

Case 1

The first experiment is carried out far from the Widom region (*p* = 15 MPa, *T*_{mean} = 31.1 °C, ΔT = 8 K, blue thermal gradient in Fig. 1). Under these conditions, the density evolves quasi linearly

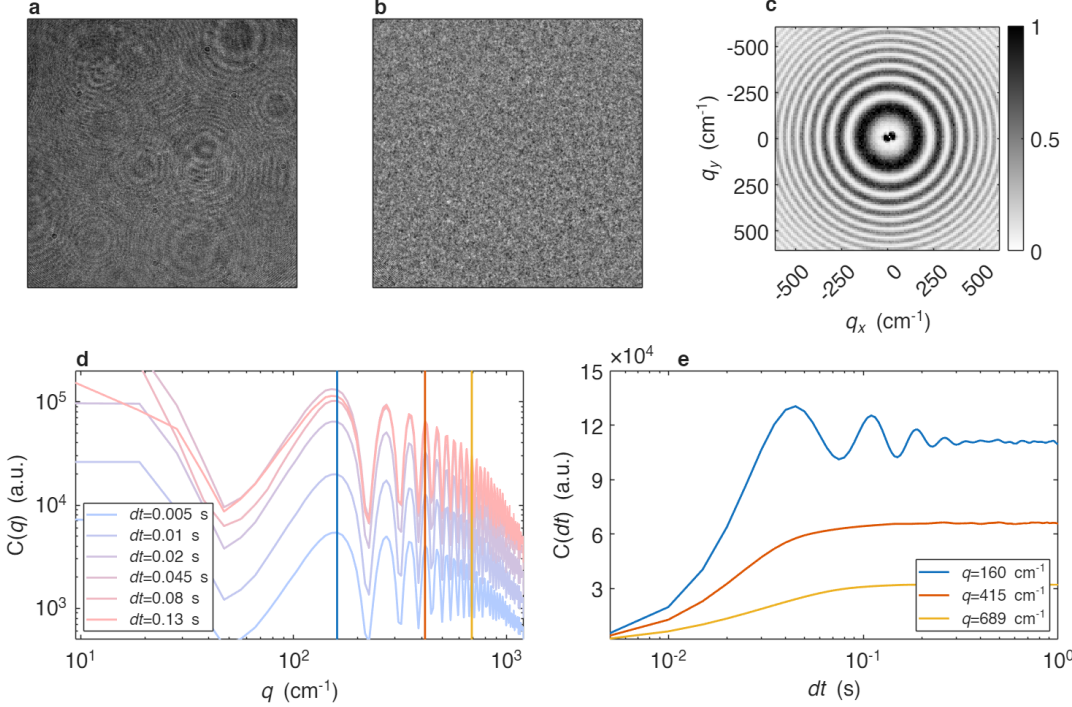


Fig. 2 Differential Dynamic Algorithm analysis of shadowgraph images. Sample data at $p = 7.5$ MPa, $T_{\text{mean}} = 31.1$ °C, $\Delta T = 4$ K. (a) Shadowgraph raw image, (b) image difference between two images acquired with a time delay $dt = 5$ s, (c) normalised 2D-structure function of the density fluctuations for $dt = 5$ s, normalised 1D-structure functions (d) for different dt from 0.005 to 0.13 s, and (e) for three different wave numbers q from 160 to 689 cm^{-1} .

and the thermal expansion coefficient is almost constant ($\Delta\beta_T \approx 1.5 \times 10^{-3}\text{K}^{-1}$, cf. Fig. 3 (a)). The resulting SFs are plotted in Fig. 3 (b). At small wave numbers, they contain one thermal mode whose amplitude is modulated by a sinusoidal function, which is the signature of a propagative mode [15, 21, 22] as described by equation (4) and as already reported for thermal and solutal fluctuations in liquid mixtures [21, 22]. The propagative mode is the result of the coupling between the thermal mode and the viscous one. The latter is not directly measurable by optical means, as it does not contribute to density fluctuations in the system, but gravity couples it to the thermal mode, producing oscillations at the mesoscopic scale within the sample for wave numbers $q < q_p$.

By fitting the structure functions over the entire range of q through the model provided by equation (4), we obtain both the time decay $\tau(q)$ and the frequency $\Omega(q)$, as reported in panels (c) and (d) of Fig. 3, respectively. For large wave number $q > q_p$, the time decay expressed

by equation (2) can be approximated by the classical thermal diffusive equation $\tau(q) = 1/(\alpha_T q^2)$ to obtain a measurement of the fluid thermal diffusivity α_T . The resulting fit is shown in panel (c) as a dark line, corresponding to a thermal diffusivity $\alpha_T = (3.9 \pm 0.1) \times 10^{-8}\text{ m}^2\text{ s}^{-1}$. For wave numbers $q < q_p$, the model for the time decay includes the kinematic viscosity, due to the coupling between the thermal mode and the viscous one. The time decay in this case can be modeled by [27] $\tau(q) = 2/[(\alpha_T + \nu)q^2]$ which provides an estimate of the fluid kinematic viscosity $\nu = (11.1 \pm 0.5) \times 10^{-8}\text{ m}^2\text{ s}^{-1}$, as shown with the dashed blue line in panel (a.iv).

Additionally, the fit of the SFs provides the values of the oscillating frequency for $q < q_p$, as shown in panel (d), from which one can estimate the maximum Brunt-Väisälä frequency $\Omega_{\text{max}} = (10.5 \pm 1) \text{ rad s}^{-1}$, and eventually the thermal expansion coefficient $\beta_T = \Omega^2/(\vec{g} \cdot \vec{\nabla} T) = (0.007 \pm 0.0013) \text{ K}^{-1}$. All the results presented until here, are coherent with those obtained in liquid binary

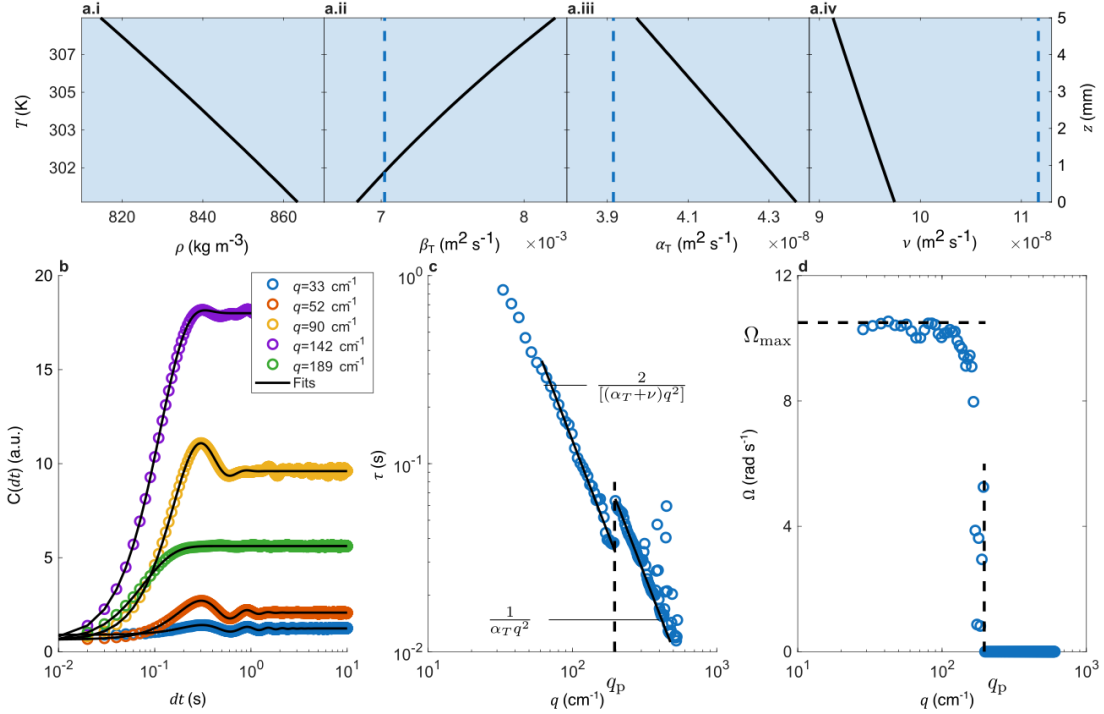


Fig. 3 Experimental results for case 1 under thermodynamic conditions far from the Widom region. Data at $p = 15$ MPa, $T_{\text{mean}} = 31.1$ °C, $\Delta T = 8$ K, blue gradient in Fig. 1. Top line: (a) thermodynamic properties of the system: (a.i) density, (a.ii) thermal expansion coefficient, (a.iii) thermal diffusivity, and (a.iv) kinematic viscosity. All the properties are plotted vs. the temperature or the height, assuming a linear relationship between the two. The temperature and height are on the vertical axis for all graphs. The vertical dotted lines show the measured data from the fitting of the SFs, as explained in the text. Bottom line: (b) 1D-Structure functions for 5 wave numbers ($33, 52, 90, 142$, and 189 cm $^{-1}$), (c) time decay $\tau(q)$ of the density fluctuations and (d) Brunt-Väisälä frequency $\Omega(q)$ as obtained by fitting the structure functions shown in (b) with the model of equation (4).

or ternary mixtures for concentration fluctuations [15, 21, 22], thus confirming the possibility of extending those results to the study of temperature fluctuations in a supercritical fluid if the non equilibrium state is far enough from the critical point or a Widom line.

Case 2

The second experiment explores thermodynamic conditions crossing the Widom region, where the thermophysical properties of the fluid are no longer linear with respect to temperature. This is achieved under the same pressure of the first experiment ($p = 15$ MPa), but with a larger thermal gradient ($T_{\text{mean}} = 40$ °C, $\Delta T = 44$ K, green gradient in Fig. 1). The resulting SFs plotted in Fig. 4(b) for different q values, show a different behaviour that cannot be captured by the model

structure function of equation (4). Therefore, a model to fit the ISF was developed and includes two distinct propagating modes, as follows

$$f(q, dt) = (1 - a) \frac{\cos[\Omega_1(q) dt + \phi_1]}{\cos(\phi_1)} \exp\left[-\frac{dt}{\tau_1(q)}\right] + a \frac{\cos[\Omega_2(q) dt + \phi_2]}{\cos(\phi_2)} \exp\left[-\frac{dt}{\tau_2(q)}\right]. \quad (7)$$

A formal demonstration of such model is outside the scope of the present Letter, however, the main idea is that a continuous superposition of modes stemming from the infinitesimal layers within the sample needs to be taken into account and the resulting ISF can be approximated by two main modes, similarly to what is done in the cumulant method [28], or in other more refined methods [29].

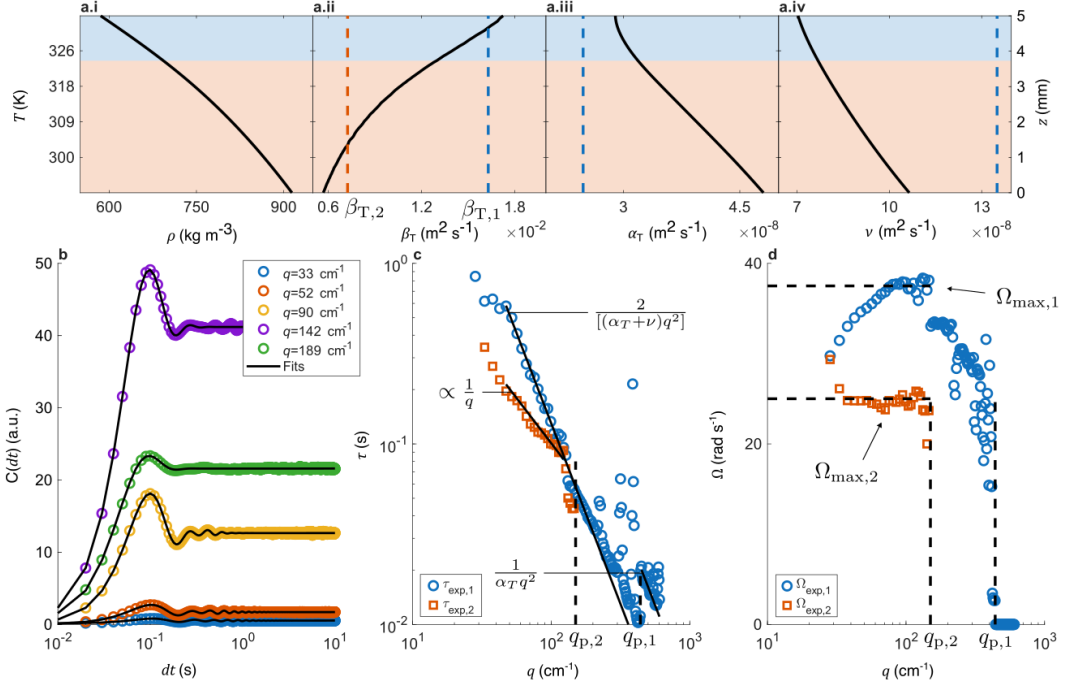


Fig. 4 Experimental results for case 2 under thermodynamic conditions crossing the Widom region. Data at $p = 15$ MPa, $T_{\text{mean}} = 40$ °C, $\Delta T = 44$ K, green gradient in Fig. 1. Top line: (a.i) density, (a.ii) thermal expansion coefficient, (a.iii) thermal diffusivity, and (a.iv) kinematic viscosity. All the properties are plotted vs. the temperature or the height assuming a linear relationship between the two. The temperature and height are on the vertical axis for all graphs. The vertical dotted lines show the measured data from the fitting of the SFs, as explained in the text. Bottom line: (b) 1D-Structure functions for 5 wave numbers (33, 52, 90, 142, and 189 cm⁻¹), (c) time decays $\tau(q)$ of the density fluctuations and (d) Brunt-Vaisälä frequencies $\Omega(q)$ as obtained by fitting the structure functions shown in (b) with the model of equation (7).

In this case, then, the fitting of the SFs provides two distinct time decays as well as two distinct oscillation frequencies, at least for a certain range of wave numbers. The resulting time decays $\tau_1(q)$ and $\tau_2(q)$ and frequencies $\Omega_1(q)$ and $\Omega_2(q)$ are presented in Fig. 4(c) and (d), respectively.

Similarly to the first experiment, the time decay $\tau_1(q)$ plotted in blue in Fig. 4(c) can be fitted for $q > q_{p,1}$ so to obtain a measurement of the fluid thermal diffusivity $\alpha_T = (2.7 \pm 0.3) \times 10^{-8}$ m² s⁻¹, a value reported in Fig. 4(a.iii). For wave numbers $q < q_{p,1}$ the fitting provides an average of the thermal diffusivity and the viscosity, from which the kinematic viscosity can be derived: $\nu = (11 \pm 2) \times 10^{-8}$ m² s⁻¹, as shown in Fig. 4(a.iv).

The time decay values $\tau_2(q)$, reported as orange squares in Fig. 4(c) for values of $q < q_{p,2}$ correspond to a second oscillatory mode and are

compatible with a sub-diffusive behaviour $\tau(q) \propto q^{-1}$ that cannot be explained according to existing models. Further analysis of this behaviour is outside the scope of this Letter.

The analysis of the frequencies reported in Fig. 4(d) reveals maximum values of $\Omega_{1,\text{max}} = (37.5 \pm 1)$ cm⁻¹ and $\Omega_{2,\text{max}} = (25 \pm 1)$ cm⁻¹. Using the same approach as above, we obtain two different values of the thermal expansion coefficient $\beta_{T,1} = (0.0163 \pm 0.001)$ K⁻¹ and $\beta_{T,2} = (0.0072 \pm 0.0006)$ K⁻¹, as reported in Fig. 4(a.ii).

The presence of two different propagating modes with different frequencies can be interpreted as a signature of fluid stratification in layers with different density gradients and, as a consequence, different β_T , which can be effectively measured using the described method. This result is particularly striking because the optical

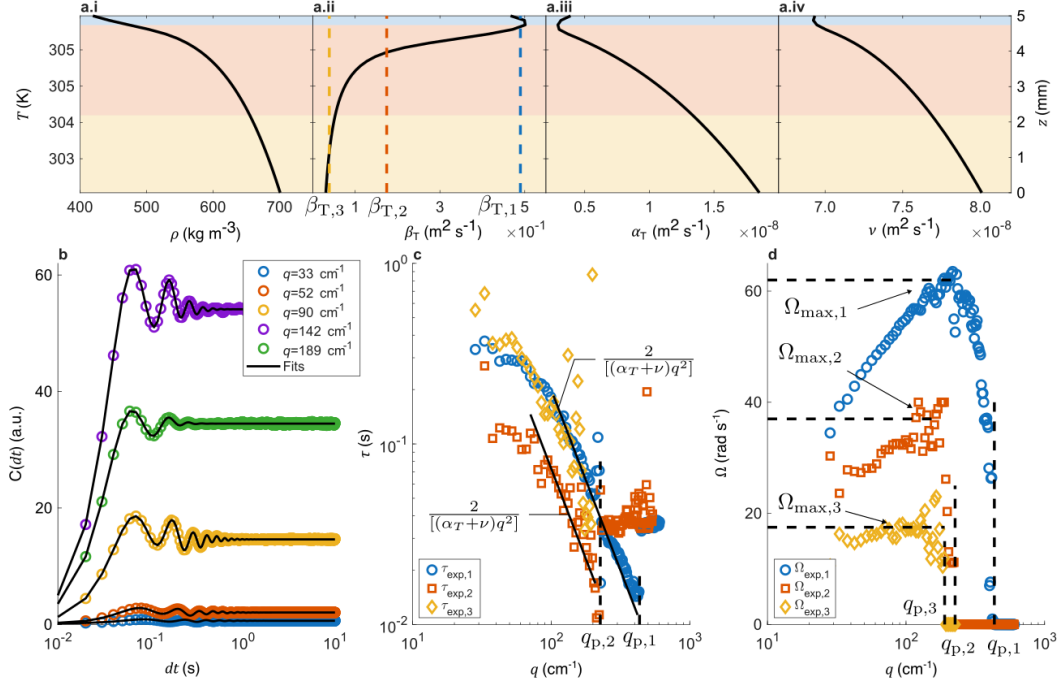


Fig. 5 Experimental results for case 3 under thermodynamic conditions crossing the Widom region, close to the critical point. Data at $p = 7.7$ MPa, $T_{\text{mean}} = 32.86$ °C, $\Delta T = 4$ K, red gradient in Fig. 1. Top line: (a) thermodynamic properties of the system inside the cell: (a.i) density, (a.ii) thermal expansion coefficient, (a.iii) thermal diffusivity, and (a.iv) kinematic viscosity. All the properties are plotted vs. the temperature or the height supposing a linear relationship between the two. The temperature and height are on the vertical axis for all graphs. Bottom line: (b) 1D-Structure functions for 5 wave numbers (66, 104, 179, 283, and 378 cm⁻¹), (c) time decay τ of the density fluctuations and (d) Brunt-Väisälä frequency Ω as obtained by fitting the structure functions shown in (b) with the model of equation (4).

method provides integrated information throughout the thickness of the fluid. Starting from the experimental values of β_T , we define two distinct volumes by choosing the separation height as the one for which averaging the theoretical values of β_T over two vertical layers separated at that height provides average β_T 's closest to the experimental values.

Case 3

Finally, we report the results of a third experiment under thermodynamic conditions closer to the critical point, $p = 7.7$ MPa, $T_{\text{mean}} = 31.1$ °C, $\Delta T = 4$ K, red thermal gradient in Fig. 1. In such conditions, the density profile is drastically non-linear, and its gradient, or equivalently β_T , shows a pronounced peak across the Widom line, as visible in Fig. 5(a.ii).

The resulting structure functions, reported in Fig. 5(b), cannot be modeled neither by one propagating mode, as in equation (4), nor by the sum of two propagating modes, as in equation (7) and an additional term is needed to obtain reasonable results from the fitting procedure, the resulting equation being similar to equation (7). In this case the fitting provides three time decays $\tau_1(q)$, $\tau_2(q)$ and $\tau_3(q)$ shown in Fig. 5(c) and three oscillation frequencies $\Omega_1(q)$, $\Omega_2(q)$ and $\Omega_3(q)$ shown in Fig. 5(d). Since fitting becomes rather complex with such a model, fitting can be performed only for $q < q_{p,1}$. As visible in the graph, the time decays $\tau_1(q)$ and $\tau_3(q)$ are essentially overlapping over a wide range of wave numbers. The fitting of their values provides, again, an average between the thermal diffusivity and the kinematic viscosity of the fluid.

The origin of such different behaviour can be better identified from the analysis of the oscillation frequencies shown in Fig. 5(d). Three distinct oscillations can be clearly identified with three different maximum frequencies, $\Omega_{1,\max} = (62 \pm 2) \text{ cm}^{-1}$, $\Omega_{2,\max} = (37 \pm 4) \text{ cm}^{-1}$ and $\Omega_{3,\max} = (17.5 \pm 1) \text{ cm}^{-1}$, corresponding to three values of $\beta_{T,1} = (0.490 \pm 0.03) \text{ K}^{-1}$, $\beta_{T,2} = (0.174 \pm 0.04) \text{ K}^{-1}$ and $\beta_{T,3} = (0.039 \pm 0.005) \text{ K}^{-1}$, as reported in Fig. 5(a.ii). These values of the density derivatives, and their comparison to the literature data, allow us to clearly identify the origin of the different oscillations in different layers, that can be referred to as a quasi-liquid layer at the bottom of the sample cell for $\beta_{T,3}$, plus two intermediate layers where β_T changes drastically, which is the signature of the transition towards a quasi-liquid phase that is not present in the volume under the reported experimental conditions. The latter interface layer, does not show any singularity of its thermophysical properties, like it happens at the (nanometric) interface of a subcritical two-phase system, but it is more a thick region where the TPs vary continuously, although strongly. This results in a vanishing, but measurable, surface tension between the two adjacent layers, an analysis beyond the scope of the current work.

These experiments reveal three main points. First, that in supercritical CO_2 , the interplay of thermal diffusion, viscosity, gravity and the presence of macroscopic gradients leads to spontaneous stratification into quasi-phases, accompanied by the signatures of distinct propagating processes in the fluctuations structure functions. Second, that in one single non-equilibrium experiment we are able to test a continuum of different points in the (P, T) phase space of the fluid system, being able to identify different quasi-states in the supercritical region. Third, that in one single non-equilibrium experiment, we are able to obtain quantitative information about the fluid transport coefficients stemming from different layers of the volume and separating them in the time (frequency) domain.

These results also help reconsider the behaviour of fluids in the supercritical and Widom regions. According to our results, the Widom region of supercritical CO_2 cannot be understood as a homogeneous state. Instead, the fluid submitted to a macroscopic temperature gradient and under the action of buoyancy,

exhibits stratified structures with quasi-phases whose properties vary dramatically. These findings challenge the conventional thermodynamic description of supercritical fluids.

The observation of multiple Brunt–Väisälä frequencies highlights a coupling between thermal and viscous modes that has no analogue in equilibrium fluids. These results suggest a new framework in which the supercritical state is viewed as an ensemble of layered quasi-phases separated by quasi-interfaces. Such a perspective has direct implications for CCUS strategies [30], energy systems exploiting supercritical CO_2 [31], and planetary sciences where non-equilibrium gradients are ubiquitous. It would be intriguing to perform a similar experiment under reduced gravity conditions, in order to check if the fluid stratification would persist. That would confirm the nature of the stratification as dominated by temperature and not by gravity. Its stability could be influenced by the presence of giant fluctuations of the temperature, and thus the density that could diverge not being damped by the buoyancy force.

Methods

Experimental setup

Experiments were conducted in a high-pressure optical cell filled with CO_2 at supercritical conditions (293.2–298.2 K, pressures above 7.4 MPa). A vertical temperature gradient was applied across the fluid layer using Peltier elements controlled with PID regulation. Density fluctuations were imaged using dynamic shadowgraphy with a superluminescent diode illumination source and a CMOS camera. Image sequences were analysed using differential dynamic analysis (DDA) [5], yielding structure functions across spatial wave numbers and time delays. Fits of intermediate scattering functions extracted characteristic decay times and Brunt–Väisälä frequencies.

Thermophysical properties

To compare our experimental values with theoretical ones, we refer to the NIST Chemistry WebBook which provides the density ρ with a precision of 0.05% [26], the specific heat mass c_p (1.5%) [26], the thermal conductivity k (2%)

[32], and the dynamic viscosity μ [33]. These literature values allow us to compute the thermal expansion coefficient $\beta_T = \frac{1}{\rho} \frac{\partial \rho}{\partial T}$ and the thermal diffusivity $\alpha_T = \frac{k}{\rho c_p}$ as a function of temperature and pressure, i.e. according to the position within the sample making the assumption of a linear temperature gradient.

Author contributions. C.G. conceived the project and P.F. and F.C. supervised it. P.F., E.L. and C.G. design and execute the experiments. P.F., H.I., C.G. and F.C. analysed and discuss the data. P.F. and F.C. wrote the paper with insights from H.I. and C.G.. P.F., E.L., H.I., C.G. and F.C. reviewed the paper. F.C. funded and administrated the project. P. Fruton: design and execution of the experiments, supervision, data analysis, paper writing, review, and editing ; E. Lisoir: execution of the experiments, paper review; H. Imuetinyan: data analysis, paper review; C. Giraudet: design and execution of the experiments, supervision, paper review, and editing; F. Croccolo: data analysis, paper writing, review, and editing, project administration, and funding acquisition.

Acknowledgements. This research was conducted within the E2S UPPA Hub Newpores and the Industrial Chair CO2ES, supported by the Investissements d’Avenir French program managed by ANR (No. ANR16IDEX0002). Fruitful discussions with Guillaume Galliero and Alberto Vailati are also acknowledged.

References

- [1] Simeoni, G.G., Bryk, T., Gorelli, F.A., Krisch, M., Ruocco, G., Santoro, M., Scopigno, T.: The Widom line as the crossover between liquid-like and gas-like behaviour in supercritical fluids. *Nat. Phys.* **6**(7), 503–507 (2010) <https://doi.org/10.1038/nphys1683>
- [2] Gallo, P., Corradini, D., Rovere, M.: Widom line and dynamical crossovers as routes to understand supercritical water. *Nat. Commun.* **5**(1), 5806 (2014) <https://doi.org/10.1038/ncomms6806>
- [3] Du, Y., Liu, L., Liao, G., Zhang, F., E., J.: Density fluctuations and transport properties of supercritical carbon dioxide calculated by molecular dynamics simulation near the Widom line. *J. Supercrit. Fluids* **200**, 106003 (2023) <https://doi.org/10.1016/j.supflu.2023.106003>
- [4] Ortiz de Zárate, J.M., Sengers, J.V.: *Hydrodynamic Fluctuations in Fluids and Fluid Mixtures*. Elsevier, Amsterdam (2006)
- [5] Croccolo, F., Bataller, H., Scheffold, F.: A light scattering study of non equilibrium fluctuations in liquid mixtures to measure the Soret and mass diffusion coefficient. *J. Chem. Phys.* **137**, 234202 (2012) <https://doi.org/10.1063/1.4771872>
- [6] Carpineti, M., Spongano, I., Croccolo, F., Vailati, A.: A cartesian diver to study oscillations and internal gravity waves in a stratified fluid. *Eur. Phys. J. E* **45** (2024) <https://doi.org/10.1088/1361-6404/ad57a2>
- [7] Fomin, Y.D., Ryzhov, V.N., Tsiok, E.N., Brazhkin, V.V.: Thermodynamic properties of supercritical carbon dioxide: Widom and Frenkel lines. *Phys. Rev. E* **91**(2), 022111 (2015) <https://doi.org/10.1103/PhysRevE.91.022111>
- [8] Mareev, E., Semenov, T., Lazarev, A., Minaev, N., Sviridov, A., Potemkin, F., Gordienko, V.: Optical Diagnostics of Supercritical CO₂ and CO₂-Ethanol Mixture in the Widom Delta. *Molecules* **25**(22), 5424 (2020) <https://doi.org/10.3390/molecules25225424>
- [9] Brazhkin, V.V., Fomin, Y.D., Lyapin, A.G., Ryzhov, V.N., Trachenko, K.: Two liquid states of matter: A dynamic line on a phase diagram. *Phys. Rev. E* **85**(3), 031203 (2012) <https://doi.org/10.1103/PhysRevE.85.031203>
- [10] Brazhkin, V.V., Lyapin, A.G., Ryzhov, V.N., Trachenko, K., Fomin, Y.D., Tsiok, E.N.: Where is the supercritical fluid on the phase diagram? *Physics-Uspekhi* **55**(11), 1061–1079 (2012) <https://doi.org/10.3367/UFNe.0182.201211a.1137>

[11] Brazhkin, V.V., Fomin, Y.D., Ryzhov, V.N., Tareyeva, E.E., Tsiok, E.N.: True Widom line for a square-well system. *Phys. Rev. E* **89**(4), 042136 (2014) <https://doi.org/10.1103/PhysRevE.89.042136>

[12] Croccolo, F., Ortiz de Zárate, J.M., Sengers, J.V.: Non-local fluctuation phenomena in liquids. *Eur. Phys. J. E* **39**, 125 (2016) <https://doi.org/10.1140/epje/i2016-16125-3>

[13] Vailati, A., Giglio, M.: q divergence of nonequilibrium fluctuations and its gravity-induced frustration in a temperature stressed liquid mixture. *Phys. Rev. Lett.* **77**, 1484 (1996) <https://doi.org/10.1103/PhysRevLett.77.1484>

[14] Vailati, A., Giglio, M.: Nonequilibrium fluctuations in time dependent diffusion processes. *Phys. Rev. E* **58**, 4361 (1998)

[15] Ortiz de Zárate, J.M., Garcia-Fernández, L., Bataller, H., Croccolo, F.: Non-equilibrium fluctuations in a ternary mixture subjected to a temperature gradient. *J. Stat. Phys.* **181**, 1 (2020) <https://doi.org/10.1007/s10955-020-02554-8>

[16] Giraudet, C., Bataller, H., Sun, Y., Donev, A., Ortiz de Zárate, J.M., Croccolo, F.: Slowing-down of non-equilibrium concentration fluctuations in confinement. *Europhys. Lett.* **111**, 60013 (2015) <https://doi.org/10.1209/0295-5075/111/60013>

[17] Croccolo, F., Brogioli, D., Vailati, A., Giglio, M., Cannell, D.S.: Effect of gravity on the dynamics of non equilibrium fluctuations in a free diffusion experiment. *Ann. N. Y. Acad. Sci* **1077**, 365 (2006) <https://doi.org/10.1196/annals.1362.030>

[18] Schmitz, R., Cohen, E.G.D.: Fluctuations in a fluid under a stationary heat flux ii. slow part of the correlation matrix. *J. Stat. Phys.* **40**, 431 (1985) <https://doi.org/10.1007/BF01017182>

[19] Law, B.M., Gammon, R.W., Sengers, J.V.: Light-scattering observations of long-range correlations in a nonequilibrium liquid. *Phys. Rev. Lett.* **60**, 1554 (1988) <https://doi.org/10.1103/PhysRevLett.60.1554>

[20] Segrè, P.N., Gammon, R.W., Sengers, J.V., Law, B.M.: Rayleigh scattering in a liquid far from thermal equilibrium. *Phys. Rev. A* **45**, 714 (1992) <https://doi.org/10.1103/PhysRevA.45.714>

[21] Croccolo, F., Garcia-Fernández, L., Bataller, H., Vailati, A., Ortiz de Zárate, J.M.: Propagating modes in a binary liquid mixture under thermal stress. *Phys. Rev. E* **99**, 012602 (2019) <https://doi.org/10.1103/PhysRevE.99.012602>

[22] Garcia-Fernández, L., Fruton, P., Bataller, H., Ortiz de Zárate, J.M., Croccolo, F.: Coupled non-equilibrium fluctuations in a polymeric ternary mixture. *Eur. Phys. J. E* **42**, 124 (2019) <https://doi.org/10.1140/epje/i2019-11889-4>

[23] Castellini, S., Brizioli, M., Giraudet, C., Carpineti, M., Croccolo, F., Giavazzi, F., Vailati, A.: Modeling and correction of image drift in dynamic shadowgraphy experiments. *Eur. Phys. J. E* **47** (2024) <https://doi.org/10.1140/epje/s10189-024-00413-y>

[24] Vailati, A., Cerbino, R., Mazzoni, S., Takacs, C.J., Cannell, D.S., Giglio, M.: Fractal fronts of diffusion in microgravity. *Nat. Commun.* **2**, 290 (2011) <https://doi.org/10.1038/ncomms1290>

[25] Giraudet, C., Bataller, H., Croccolo, F.: High-pressure mass transport properties measured by dynamic near-field scattering of non-equilibrium fluctuations. *Eur. Phys. J. E* **37**(11), 107 (2014) <https://doi.org/10.1140/epje/i2014-14107-1>

[26] Span, R., Wagner, W.: A new equation of state for carbon dioxide covering the fluid region from the triple-point temperature to 1100 k at pressures up to 800 mpa. *J. Phys. Chem. Ref. Data* **25**, 1509–1596 (1996) <https://doi.org/10.1063/1.555991>

[27] Wu, W., Jander, J.H., Rausch, M.H., Fröba,

A.P., Giraudet, C.: Simultaneous determination of multiple transport properties over a wide range of temperatures and pressures from the analysis of non-equilibrium fluctuations by the shadowgraph method. *J. Chem. Phys.* (153), 144201 (2020) <https://doi.org/10.1063/5.0024503>

[28] Mailera, A.G., Clegg, P.S., Pusey, P.N.: Particle sizing by dynamic light scattering: Non-linear cumulant analysis. *J. Phys.: Condens. Matter* **27**, 145102 (2015) <https://doi.org/10.1088/0953-8984/2>

[29] Castellini, S., Carpineti, M., Giraudet, C., Croccolo, F., Vailati, A.: Dynamics of non-equilibrium concentration fluctuations during free-diffusion in highly-stratified solutions of glycerol and water. *J. Chem. Phys.* **158**, 244201 (2023) <https://doi.org/10.1063/5.0151752>

[30] Imre, A.R., Ramboz, C., Deiters, U.K., Kraska, T.: Anomalous fluid properties of carbon dioxide in the supercritical region: application to geological CO₂ storage and related hazards. *Environ. Earth Sci.* **73**(8), 4373–4384 (2015) <https://doi.org/10.1007/s12665-014-3716-5>

[31] Ren, J., Marxen, O., Pecnik, R.: Boundary-layer stability of supercritical fluids in the vicinity of the Widom line. *J. Fluid Mech.* **871**, 831–864 (2019) <https://doi.org/10.1017/jfm.2019.348>

[32] Huber, M.L., Sykioti, E.A., Assael, M.J., Perkins, R.A.: Reference correlation of the thermal conductivity of carbon dioxide from the triple point to 1100 k and up to 200 mpa. *J. Phys. Chem. Ref. Data* **45** (2016) <https://doi.org/10.1063/1.4940892>

[33] Laeisecke, A., Muzny, C.D.: Reference correlation for the viscosity of carbon dioxide. *J. Phys. Chem. Ref. Data* **46** (2017) <https://doi.org/10.1063/1.4977429>